PERGAMON

Scripta mater. 42 (2000) 1179–1186

Scripta MATERIALIA

www.elsevier.com/locate/scriptamat

COUPLING OF MULTICOMPONENT THERMODYNAMIC DATABASES TO A PHASE FIELD MODEL: APPLICATION TO SOLIDIFICATION AND SOLID STATE TRANSFORMATIONS OF SUPERALLOYS

U. Grafe, B. Böttger, J. Tiaden and S.G. Fries
ACCESS e. V., Intzestraße 5, D-52056 Aachen, Germany

(Received November 4, 1999)
(Accepted January 13, 2000)

Keywords: Nickel; Thermodynamics; Microstructure; Phase transformation; Simulation

Introduction

The phase field method has successfully been applied to predict microstructure evolution in metallic alloys such as dendritic solidification [1,2,3] as well as the precipitation of coherent ordered phases from a disordered matrix taking into account the effect of elastic strain on the morphology of the precipitates [4,5,6]. Recently, phase field methods employing multiple phase field parameters have been applied to eutectic and peritectic systems [7,8,9] in dilute model systems as well as to evaluate the kinetics of solid state grain growth [10]. In order to apply the method quantitatively to these phenomena occurring in technical alloys the method needs to be able to treat multicomponent multi-phase systems. Recently a simplified multicomponent approach using linearized phase diagrams has been applied to steels [11]. The ternary system Fe-Al-Co has been addressed by [5] who use real thermodynamic data within a phase field model. The main target of this work is to simulate solidification and heat treatment of technical single crystal superalloys.

The present paper proposes a multicomponent extension to a multi-phase-field model (PFM) described in [12,13] employing a general method of obtaining thermodynamic data from databases being assessed according to the CALPHAD method [14]. This method provides realistic thermodynamic descriptions for all phases present in a given material. The present model can be applied to any system if a thermodynamic database is available and is not restricted to a special formulation of the Gibbs energy. To evaluate thermodynamic quantities the FORTRAN interface of the software Thermo-Calc [15] is used for the calculation of molar Gibbs energies and chemical potentials to calculate the driving force at the diffuse interface. Furthermore, a subroutine of the software Dictra [16], which is also interfaced to Thermo-Calc in order to calculate thermodynamic factors of diffusion, has been coupled to the phase field code. The subroutine calculates the diffusion matrix for given multicomponent phase from a standardized kinetic database containing data on atomic mobilities.

In order to validate the growth kinetics of this model 1D benchmark tests have been performed by comparison with a sharp interface calculation by Dictra using the same thermodynamic [17] and kinetic database [18] of the ternary Ni-Al-Cr system. Moreover, a 2D simulation of Ostwald-ripening of spherical γ' precipitates in a ternary Ni-Al-Cr alloy with a small γ-γ' lattice mismatch is presented. The results are compared to experimental data by M. Doi [19], who determined the coarsening rate of the γ' precipitates in a Ni-6.2 at.-% Al-18.2 at.-% Cr alloy.

PII S1359-6462(00)00355-9

The Multi-Phase-Field Model

The multi-phase-field model is described in detail in [12,13]. The evolution of the phase field ϕ_i for a phase i with respect to time is given for a double well potential by:

$$\dot{\phi}_i = \sum_j^N \mu_{ij} \left[\sigma_{ij} \left(\phi_i \nabla^2 \phi_j - \phi_j \nabla^2 \phi_i + \frac{36}{\eta_{ij}^2} \phi_i \phi_j (\phi_i - \phi_j) \right) + \frac{6}{\eta_{ij}} \phi_i \phi_j \cdot \Delta G_{ij} \right] \quad (1)$$

(μ_{ij}: mobility, η_{ij}: interface thickness, N: number of phases, ΔG: change in Gibbs energy for the transformation of phase i to j, the negative driving force). In the sharp interface limit this phase field equation in principle models the normal velocity v_n of the interface between phases i and j

$$v_n = \mu_{ij} (\Delta G_{ij}^{interface} + \Delta G_{ij}^{bulk}) \quad (2)$$

where $\Delta G_{ij}^{interface}$ represents the product of the interfacial energy σ_{ij} and the curvature κ. Usually the driving force resulting from the difference in Gibbs free energy of the bulk phases ΔG_{ij}^{bulk} for low undercoolings ΔT is approximated by

$$\Delta G_{ij} = \frac{\Delta H_{ij}^0}{T_{ij}^0} (T_{ij}^0 - T) = \Delta S_{ij}^0 \Delta T_{ij} \quad (3)$$

for a transformation from phase i to j under the assumption that T is so close to the equilibrium temperature T_{ij}^0 that the variation of the enthalpy ΔH_{ij}^0 and entropy ΔS_{ij}^0 with T is negligible. This approximation of the driving force is applicable for low undercoolings of pure substances and dilute solutions, but not for concentrated alloys. This value ΔG_{ij} is the negative value of the integrated driving force which is independent of the reaction path [20]. In order to generalize this expression for multicomponent alloys we have to evaluate the driving force $D = -(\partial G/\partial \xi)_{P,T,ni}$ which can be the partial derivative of the Gibbs free energy with respect to a variable ξ which represents the extent of an internal reaction [20]. In the case of the precipitation of a phase j from an initially supersaturated solution of a phase i, the variable ξ represents for the number of moles n^j of the precipitated phase formed. The integrated driving force being the integral of the driving force $\int D\, d\xi$ is an average value of the whole precipitation process. It represents the difference in Gibbs energy of the final mixture of phases i and j lying on the common tangent plane and the molar Gibbs energy of the initially supersaturated solution. In contrast to this we choose the negative driving force ΔG_{ij} of the supersaturated solution as the appropriate value, since this is the local driving force which acts on the interface: The interface and the actual concentration within the interface do not see their final state on the path to equilibrium, but they are driven by the local win of Gibbs energy on this path. So the movement of the interface will be suppressed, if the local driving force on this path would be negative, even if there is globally an equilibrium state with lower energy. For a multicomponent system this value per mole phase j is given by, Fig. 1 [20]:

$$\Delta G_{ij} = G_j^{molar} (c_j^k) - \sum_{k=1}^N c_j^k \mu_i^k (c_i^k) \quad (4)$$

(c_i^k: concentration, i.e. mole fraction of component k in phase i, μ_i^k: chemical potential of component k in phase i, G_j^{molar}: molar Gibbs energy of phase j). This expression is calculated from the local compositions of both phases, which have to be evaluated from an overall mixture concentration c^k for component k:

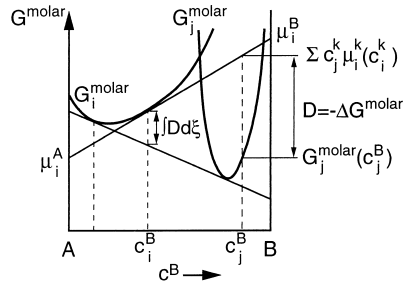

Figure 1. Thermodynamic driving force on an interface of a phase j growing from a matrix phase i.

$$c^k(\vec{x},t) = \sum_{i=1}^{N} \phi_i(\vec{x},t) c_i^k(\vec{x},t) \tag{5}$$

The concentrations c_i^k are substituted using the equilibrium partition coefficients k_{iR}^k of a phase i to a reference phase R which is chosen arbitrarily. The partition coefficients are calculated dependant on composition and temperature using the TQ-Interface of Thermo-Calc. We obtain the compositions of a phase i from the mixture concentrations c^k:

$$c_i^k = k_{iR}^k c^k / \sum_{j=1}^{N} \phi_j k_{ij}^k \tag{6}$$

The multi-phase diffusion equation for the mixture concentration of component k is given by:

$$\dot{c}^k(\vec{x},t) = \nabla(\sum_{i=1}^{N} \phi_i j_i^k) \tag{7}$$

The density of the diffusional flux j_i^k of a component k according to the Fick-Onsager equation expressed in terms of diffusivities and concentration gradients rather than mobilities ${}_i\boldsymbol{L}_{kj}$ and gradients of the chemical potentials [16] is given for an alloy containing n components:

$$j_i^k = \sum_{l=1}^{n}{}_i\boldsymbol{L}_{kj} \nabla \mu_i^l = -\sum_{l=1}^{n-1}{}_i\boldsymbol{D}_{kj}^n \nabla c_i^l \tag{8}$$

The reduced diffusion matrix ${}_i\boldsymbol{D}_{kj}^n$ for phase i is calculated by a subroutine of the Dictra software.

Benchmark with 1D Sharp Interface Calculations

The sharp interface calculations are carried out using the Dictra software. The binary Ni-Al system has been chosen for this benchmark test. Kinetic data for the γ' phase are not available and therefore diffusion in this phase is not taken into account. The growth of the γ' phase is simulated starting from T = 1500 K cooling down to 1300 K in 200 s with a constant cooling rate. The following parameters have been adjusted: grid resolution $\Delta x = 5$ nm (Dictra: $\Delta x = 10$ nm), interface thickness: $\eta = 30$ nm, $\mu = 0.64$ s. In general, the phase field mobility μ for diffusion controlled transformations is no adjustable parameter and has to be chosen in a way that the value has no impact on the kinetics. The

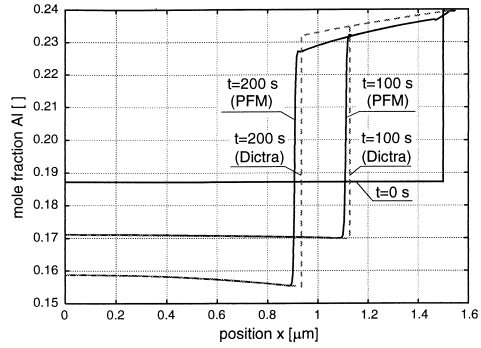

Figure 2. Concentration profiles of Al in γ and γ' calculated using the PFM and Dictra.

interfacial energy is estimated to $\sigma = 2$ mJ/m^2. However, since the simulation is 1D, i.e. curvature effects are not included, this value just affects numerical stability rather than the growth kinetics. The concentration profiles for t = 100 s and t = 200 s are presented in Fig. 2. In general, the PFM calculation reproduces the result from Dictra apart from a mass balance error resulting in a too small γ' composition at the interface. This is due to a simplified numerical implementation of the partition coefficients in order to save calculation time and will be minimized in updated algorithms.

A second calculation compares the results of the PFM and Dictra for solidification at a cooling rate of 0.1 K/s starting from 1688.4 K in the ternary Ni-Al-Cr system. In case of solidification simulations usually the solidified part of the calculation domain is identified with the half of a secondary dendrite arm, which is assumed to be plate-like. Since no accurate diffusivities are available for the liquid phase the values are set constant ($D^{liq} = 10^{-9}$ m^2/s) for both alloying elements. The grid resolution is chosen to be $\Delta x = 1$ μm for both calculations and $\eta = 4$ μm for the interface thickness.

The concentration profiles of the elements Al and Cr for four different time steps are presented in Fig. 3a,b. Compared to the γ' calculation the results of the solidification simulation are in a better agreement due to the fact that the temperature range of 6 K is much smaller. This leads to a smaller variation in the partition coefficient and thus a more accurate reproduction of the tielines at the liquid-γ interface. While off-diagonal terms of the diffusion matrix are not implemented in the PFM code the full diffusion matrix is taken into account by Dictra. However, this does not affect the result, since diffusion in the solid does not play any role under the given conditions.

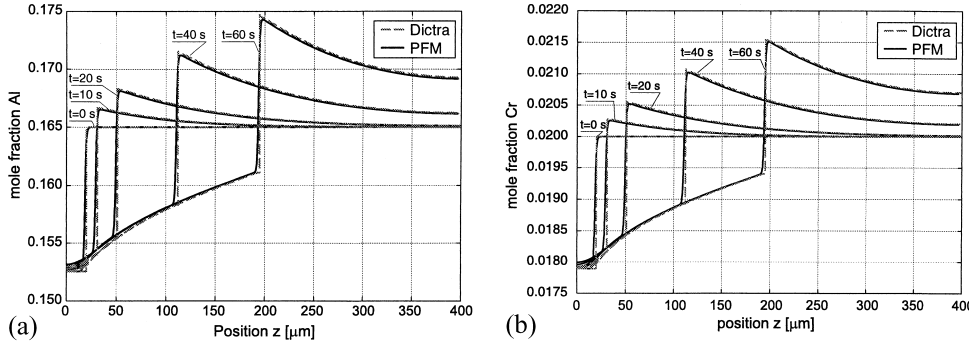

Figure 3. a: Calculated concentration profiles of Al system during solidification in the Ni-Al-Cr system. b: Calculated concentration profiles of Cr system during solidification in the Ni-Al-Cr system.

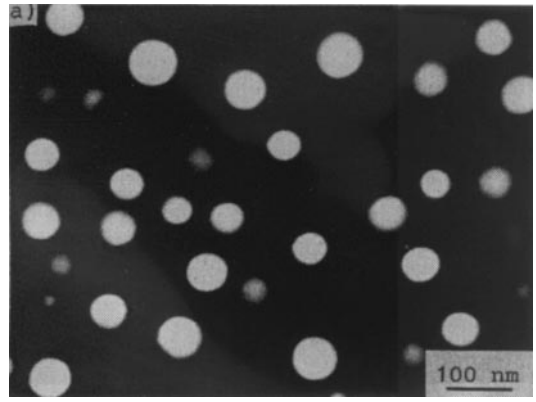

Figure 4. TEM micrograph of the sample presented in [16] after 86400 s.

2D Ostwald-Ripening of Spherical γ' in a Ni-Al-Cr Alloy

This numerical example was intended to simulate an experiment carried out by M. Doi [19] who examined the impact of the γ/γ' lattice mismatch on coarsening. The alloy Ni-18.2at.%Cr-6.2at.%Al, which contains spherical γ' precipitates, was aged at 1073 K for 691000 s. A given TEM-micrograph of the specimen quenched after 86400 s was used to set the initial condition for the phase field calculation, Fig. 4,5. However, the calculation of the equilibrium compositions using available databases [17,21] for both phases yielded that the γ' phase is not stable for the given alloy composition. Some further equilibrium calculations for Ostwald-ripening experiments in Ni-Al-Cr alloys summarized in [21] yield similar results, i.e. that γ' is not stable. In order to perform a reasonable simulation despite of these uncertainties, the marked tieline in Fig. 8 was selected as the operating tieline for this experiment. The high Cr content in the γ' phase reduces the lattice mismatch due to the lower atomic radius of Cr compared to Al. This should lead to spherical precipitates instead of cuboidal ones. The following parameters have been chosen: $\Delta x = 3$ nm, $\mu = 1600$ s, $\eta = 12$ nm. The diffusion coefficients in the matrix are in $m^2\ s^{-1}$: $D_{Al} = 2.1 \cdot 10^{-17}$, $D_{Cr} = 5.3 \cdot 10^{-18}$. The interfacial energy $\sigma = 6.9\ mJ/m^2$ was taken from a binary Ni-Al alloy [23] neglecting the dependency on composition and temperature. Moreover, no diffusion in the γ' phase and constant diffusion coefficients are assumed. The off-diagonal terms of the diffusion matrix are not taken into account.

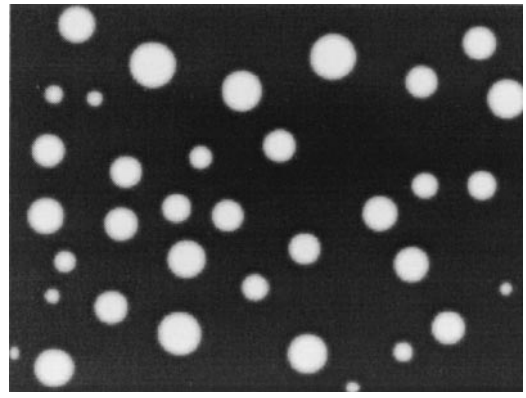

Figure 5. Initial distribution of γ' particles (light circles) for the phase field simulation.

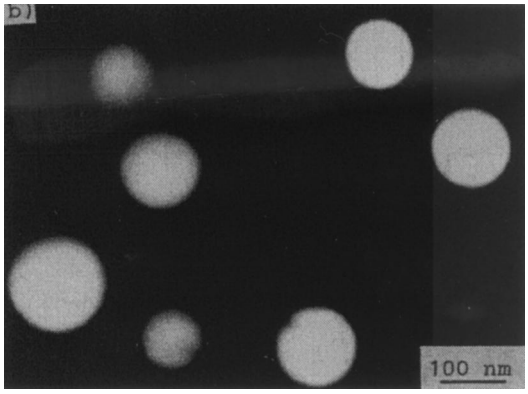

Figure 6. TEM micrograph of the sample after 691000s of aging (at a different position).

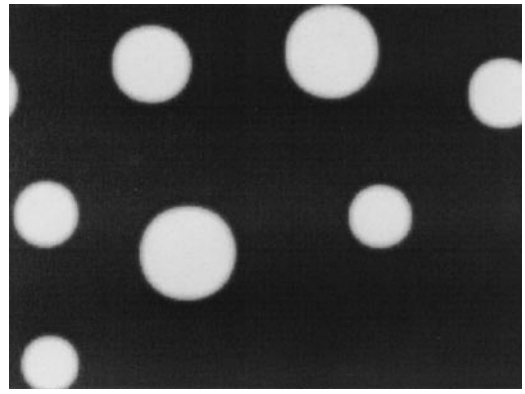

Figure 7. Simulated microstructure after 691000s.

A TEM-image of the microstructure and the simulated counterpart are shown in Fig. 6, 7. The third power of the mean radius of the precipitates as a function of time is presented in Fig. 9. Despite of the still crude treatment done for this alloy, the deviation between measured mean radius (61.2 nm) and the calculated value (58.5 nm) as well as the growth rate (both $k = 0.3\ m^3\ s^{-1}$) are small. Since the simulation is 2D, the growth rate for a 3D calculation must be multiplied by a factor of at least 2 resulting from a different ratio of surface to volume of circle and sphere. This leads to the conclusion that calculated and measured values are of the same order of magnitude.

Summary and Outlook

A multicomponent multi-phase-field model has been developed. 1D benchmark tests with the software Dictra have been carried out to demonstrate that the model reproduces the right growth kinetics of diffusion controlled phase transformations in multicomponent systems. Compared to Dictra the phase field model moreover allows for 2D and 3D calculations taking into account complex morphologies including effects of curvature. A 2D simulation of Ostwald-ripening in a ternary alloy has been being

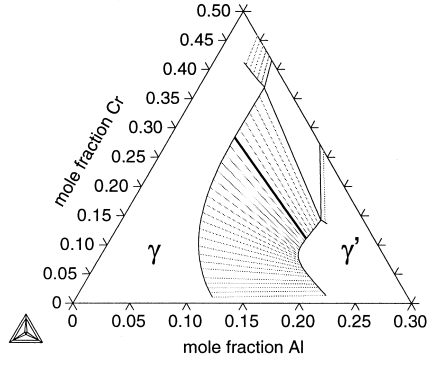

Figure 8. Isothermal section calculated for 1073K. The marked tieline was used for the 2D simulation of Ostwald-ripening.

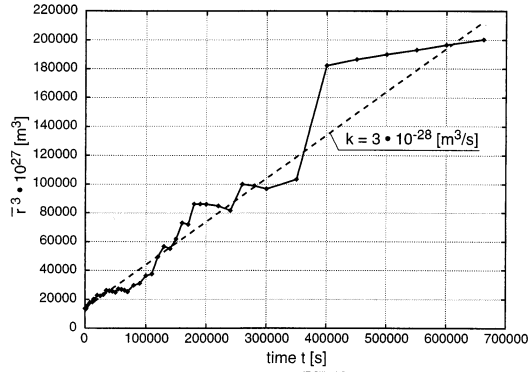

Figure 9. Calculated evolution of the mean radius of γ' as a function of time.

compared to experimental data. Calculated and experimentally determined growth rates are of the same order of magnitude. These results principally show the feasibility quantitative phase field simulations of diffusion controlled phase transformations in technical alloys.

A full treatment of the Fick-Onsager equations will be implemented soon and additional benchmarks will be carried out for alloys, in which cross diffusion cannot be neglected. The model has not been applied to multi-phase and multiple order parameter systems in this work. Future work will apply the model to phase transformations in polycrystalline materials, e.g. the precipitation of ferrite from an austenitic matrix in steels. Continuing the work on superalloys, spatially resolved simulations of dendritic solidification and the growth of cubic γ' taking into account the effect of coherency strain will be carried out.

Acknowledgments

The authors gratefully acknowledge the financial support of the Deutsche Forschungsgemeinschaft (DFG) within the Collaborative Research Center 370 “Integrated Modeling of Materials.” The authors would like to thank Prof. Dr. B. Sundman and Dr. L. Höglund for their support concerning the implementation of thermodynamic and kinetic data within the phase-field model.

References

1. J. A. Warren and W. J. Boettinger, Acta Metall. Mater. 43(2), 689 (1995).
2. J. Tiaden and U. Grafe, in Proceedings of the International Conference on Solid-Solid Phase Transformations ’99, Kyoto, 1999, to be published.
3. J. F. McCarthy, Acta Metall. Mater. 45(10), 4077 (1995).
4. Y. Wang, D. Banerjee, C. C. Su, and A. G. Khachaturyan, Acta Metall. Mater. 46(9), 2983 (1998).
5. T. Miyazaki, T. Koyama, and T. Kozakai, Mater. Res. Soc. Symp. Proc. 481 (1998).
6. D. Y. Li and L. Q. Chen, Acta Mater. 45, 2435 (1997).
7. A. A. Wheeler and G. B. McFadden, Proc. R. Soc. Lond. Ser. A 453, 1611 (1997).
8. M. Seeßelberg, J. Tiaden, G. J. Schmitz, and I. Steinbach, Proceedings of Solidification Processing, Sheffield, 1997.
9. J. Tiaden, J. Crystal. Growth. 198/199, 1275 (1999).
10. D. Fan and L. Q. Chen, in Mathematics of Microstructure Evolution, ed. L. Q. Chen, B. Fultz, J. W. Cahn, J. R. Manning, J. E. Morral, and J. A. Simmons, The Minerals, Metals & Materials Society, Pittsburgh, PA (1996).
11. J. Tiaden, U. Grafe, and B. Böttger, Proceedings of Euromat ’99, to be published.
12. I. Steinbach, F. Pezzolla, B. Nestler, M. Seeßelberg, R. Prieler, G. J. Schmitz, and J. L. L. Rezende, Phys. D. 94, 135 (1996).

13. J. Tiaden, B. Nestler, H. J. Diepers, and I. Steinbach, Phys. D. 115, 73 (1998).
14. N. Saunders and A. Miodownik, Elsevier Science Ltd., Amsterdam (1998).
15. B. Sundman, B. Jansson, and J. O. Anderson, CALPHAD 9. 2, 153 (1985).
16. A. Engström, L. Höglund, and J. Ågren, Metall. Trans. 25A, 1127 (1994).
17. N. Saunders, in Superalloys 1996, eds. R. D. Kissinger, et al., p. 101, TMS, Warrendale, PA.
18. A. Engström and J. Ågren, Z. Metallkunde. 87(2), 92 (1996).
19. M. Doi and T. Miyazaki, in Superalloys 1988, eds. S. Reichman, D. N. Duhl, G. Maurer, S. Antolovich, and C. Lund, pp. 663–671, The Metallurgical Society (1988).
20. M. Hillert, Phase Equilibria, Phase Diagrams and Phase Transformations: A Thermodynamic Basis, Cambridge University Press.
21. N. Dupin, Ph.D. Thesis, Laboratoire de Thermodynamique et de Physico-Chimie Métallurgique de Grenoble, 1995.
22. C. S. Jaynath and P. Nash, J. Mater. Sci. 24, 3041 (1989).
23. A. Ardell, Interface Sci. 3, 119 (1995).